International Journal of Hydrogen Energy 111 (2025) 567–580

Contents lists available at ScienceDirect

International Journal of Hydrogen Energy

journal homepage: www.elsevier.com/locate/he

Supercritical water gasification and subsequent steam reforming of the product gas under elevated temperature and pressure

Athanasios A. Vadarlis [a,*], Dominik Neukum [a], Julian Dutzi [a], Angeliki A. Lemonidou [b,c], Nikolaos Boukis [a], Jörg Sauer [a]

[a] Karlsruhe Institute of Technology (KIT), Institute of Catalysis Research and Technology (IKFT), Hermann-von-Helmholtz-Platz 1, 76344, Eggenstein-Leopoldshafen, Germany
[b] Aristotle University of Thessaloniki (AUTH), Department of Chemical Engineering, University Campus, GR-54124, Thessaloniki, Greece
[c] Chemical Process Engineering Research Institute (CERTH/CPERI), P.O. Box 6036, Thermi, Thessaloniki, 57001, Greece

ARTICLE INFO

Handling Editor: Dr J Lobato

ABSTRACT

A continuous process combining the supercritical water gasification (SCWG) of ethanol with the subsequent steam reforming (SR) of the product gas was investigated. An experimental study was conducted that involved the operating parameters in the SR reactor, the ethanol concentration, and a comparison of two commercial catalysts for SR. With ethanol as a biomass model compound, complete gasification in the SCWG reactor was achieved. Regarding the SR reactor, high pressures, i.e., 20–40 bar, required a temperature of 750 °C to achieve methane conversion higher than 90% at a constant gas hourly space velocity of 63500 h^{-1}. The increase in EtOH concentration significantly decreased the steam/carbon ratio of the SCWG product and increased the content of CH_4, C_{2+} hydrocarbons, and CO. This in turn resulted in a decrease in H_2 yield in the SR reactor from 98.6% to 58.3%, as the EtOH concentration increased from 5 wt% to 20 wt% at a temperature of 730 °C, pressure of 30 bar, and a space velocity of 47877 h^{-1}. Under atmospheric pressure, both catalysts showed similar CH_4 conversion. However, at higher pressures (30–40 bar), the catalyst with the higher Ni loading exhibited greater activity in SR.

1. Introduction

In order to address climate change, recent global policies are encouraging a shift from fossil fuels to sustainable energy sources and the capture and use of CO_2 as a carbon resource [1–3]. Hydrogen production has become one of the most important means to this end, with hydrogen serving both as an energy carrier [4–6] and as a raw material, together with the CO_2, for the petrochemical, chemical, and the metal industry [7,8].

The conventional technology for the production of hydrogen in industrial scale is the steam reforming of natural gas. There, the Steam Methane Reforming (SMR) reaction takes place at high temperatures (800–900 °C), pressures in the range of 20–30 bar, and H_2O/CH_4 ratios of 2.5–3 [7,9,10], producing H_2 and CO.

$$CH_4 + H_2O \leftrightarrow 3H_2 + CO, \Delta H_{298K} = 206 \frac{kJ}{mol} \quad (1)$$

If heavier hydrocarbons are present in the feed, they are also reformed in a catalytic reactor installed upstream of the main reformer, called pre-reformer (according to equation (2)) [11,12].

$$C_nH_m + H_2O \rightarrow CO + \left(\frac{m}{2} + n\right)H_2 \quad (2)$$

($\Delta H_{298K} \approx 150n + 50$ kJ mol^{-1} for linear hydrocarbons [11]). The product from the reformer is driven to two shift reactors, where CO reacts with H_2O to produce CO_2 and H_2, according to the Water Gas Shift (WGS) reaction (equation (3)).

$$CO + H_2O \leftrightarrow H_2 + CO_2, \Delta H_{298K} = -41 \frac{kJ}{mol} \quad (3)$$

However, this process has a very high carbon footprint unless a CO_2 capture facility is integrated into it, producing what is known as blue hydrogen [7]. Other biofuels, such as ethanol, methanol, or glycerol, can be reformed with steam in thermochemical recuperation systems [13–15]. In this way, the steam reforming process can become a more sustainable technology. However, the steam reforming of biofuels is

* Corresponding author.
E-mail address: athanasios.vadarlis@kit.edu (A.A. Vadarlis).

https://doi.org/10.1016/j.ijhydene.2025.02.197
Received 12 November 2024; Received in revised form 30 January 2025; Accepted 12 February 2025
Available online 26 February 2025

constrained by the limited availability of suitable feedstocks, as it cannot effectively process more complex biomass-based materials. In the future, the primary production technology of hydrogen will be water electrolysis [16,17], but a disadvantage of this technology which remains yet to be solved is its high energy demand [18,19]. An alternative sustainable solution is the gasification of waste biomass. The gasification of biomass can be achieved via steam, air, or supercritical water [20]. Using supercritical water for biomass gasification is particularly effective for processing waste biomass with high water content, as it eliminates the need for feed pre-drying [21], unlike the gasification technologies that use other gasifying agents. The product from this process contains a relatively high molar fraction of hydrogen, allowing thus an easier separation from the rest of the product gases [20].

Under supercritical conditions (T > 374 °C, P > 221 bar), water faces a dramatic decrease in its density, viscosity, and dielectric constant, being able to dissolve non-polar organic substances, and facilitate their hydrolysis, turning them to their monomers [18,22]. These monomers react then with water to generate H_2, CO, and CO_2 [21] (equations (4) and (5)). Carbon monoxide reacts with H_2 to form CH_4 via the reverse SMR reaction and with steam via the WGS reaction [23]. Methane can also be formed by other reactions, such as by decarboxylation of acetic acid or by decarbonylation of acetaldehyde [24].

$$C_xH_yO_z + (2x - z)H_2O \rightarrow xCO + \left(x - z + \frac{y}{2}\right)H_2 \quad (4)$$

$$C_xH_yO_z + (2x - z)H_2O \rightarrow xCO_2 + \left(2x - z + \frac{y}{2}\right)H_2 \quad (5)$$

Depending on the operating conditions of SCWG, the catalysts, and the biomass structure, additional chemical reactions may occur, which generate coke, tars, and heavier hydrocarbons [18,25–27].

A recent review on the catalytic supercritical water gasification (SCWG) of actual biomass and model compounds revealed that, in most instances, a substantial portion of the hydrogen produced (approximately 30%) was bound to hydrocarbons, primarily methane [28]. The hydrocarbons can be converted to H_2 and carbon oxides in a downstream steam reforming (SR) reactor [26,29].

To date, several studies have worked on developing and simulating processes that combine biomass SCWG with SR of the product gas [30–33] or even methane dry reforming, for increased hydrogen production [34,35]. However, to the best of the authors knowledge, there has not been any experimental work on combining these two processes.

Recently, the authors of this work demonstrated a continuous laboratory-scale process for the combined SCWG of ethanol (EtOH) acting as a biomass model compound, with subsequent steam reforming of the resulting hydrocarbons in the presence of a Ni-based catalyst (18 wt% NiO) supported on a $CaK_2Al_{22}O_{34}$ support [28]. The gasification of 8 wt% EtOH (in water) was conducted at 600 °C and 250 bar. The SCWG product gas, after decompression to pressures ranging from 1 to 40 bar, together with the remaining steam from the gasification, entered the second reactor, where SR of the produced hydrocarbons was conducted on a commercial Ni-based catalyst. It was found that the integration of the reformer, operating under atmospheric pressure, 600 °C and with a gas hourly space velocity (GHSV) of 14850 h^{-1}, increased the hydrogen yield based on the EtOH in the feed from 27.4% (only with SCWG) to 98%. The excess steam resulted in very high steam/carbon (S/C) ratios, inhibiting carbon formation on the catalyst but accelerating the sintering of the active metal. Other similar experimental studies could not be found in the literature.

The purpose of this work was to further investigate the effect of various parameters on the hydrogen yield and the conversion of hydrocarbons to elemental hydrogen. More specifically, the influence of temperature, pressure and space velocity were investigated by applying a new catalyst to the reformer, a Ni-based one with a support of $CaAl_{12}O_9$ and with a loading of 14 wt% NiO. The new catalyst was then compared with the catalyst applied in the previous study. Furthermore, a new parameter investigated was the concentration of EtOH in the feed and how this affects the intermediate SCWG gas product and the final one following the tandem steam reforming step. Compared to the previous publication [28], the focus in the present work was on temperature and pressure in the second reactor that are relevant to those applied on an industrial scale for hydrocarbons steam reforming.

2. Experimental methods

2.1. Experimental setup

The feeding system comprises a scale, a vessel with an EtOH/water solution, and an HPLC pump (Bischoff Model 2250). A capillary tubing connects the pump outlet to the SCWG reactor entrance. The SCWG reactor (I) is made of nickel-based alloy 625, measuring 1000 mm in length and 8 mm in inner diameter. Heat is supplied to reactor I through three spiral heating coils on the outer wall. Six thermocouples monitor and regulate the temperature across the reactor's outlet. The heated part of this reactor was 650 mm long. The pressure is controlled by a back-pressure regulator (Equilibar, ULHT Series Precision, Pressure Control Solutions) capable of operating at temperatures up to 500 °C, set at 265 bar. A heating coil maintains the temperature around 500 °C in the pipe between the SCWG reactor and the pressure regulator, preventing phase separation.

The pre-heater (II) is positioned downstream of the back-pressure regulator, connected to its outlet port. This nickel-based alloy 625 rod is 800 mm long with an 8 mm inner diameter. It is equipped with three heating coils.

After the pre-heater, the SCWG product gas is driven to the SMR reactor (Reactor II). The SMR has a length of 880 mm and an 8 mm inner diameter and is a Ni-based alloy 602. A heating coil welded on the outer surface of the reactor keeps the reactor heated at temperatures up to 800 °C. The fixed catalytic bed is located in the center of the reactor. A thermocouple coming from the entrance of the reactor via a t-piece connection measures the temperature of the catalytic bed. The catalytic bed consists of the catalyst particles (250–500 μm) supported by a metallic net and quartz wool. The catalysts used are the commercially available ReforMax 330 LDP and ReforMax 210 LDP (R330 and R210, respectively), purchased from C&CS catalysts and chemicals specialties GmbH. The nominal NiO content of R330 is 14 wt% and the rest is a $CaAl_{12}O_9$ support, while the R210 has 18 wt% NiO supported on $CaK_2Al_{22}O_{34}$.

The product stream from the SMR passes through a gas sampling bulb, a liquid-gas separator, and a gas meter (type TG0.5/7, provided by Ritter), after depressurization by a Tescom back-pressure regulator. The liquid condensate is collected in the phase separator and its weight is measured by a scale. Fig. 1 depicts the system described above. An intermediate gas sampling point consisting of three valves (V02, V03, V04) and a gas bulb are installed for measuring the product gas composition from the first reactor.

2.2. Experimental procedure

Before the experiments, an H_2(20 vol%)/N_2 gas was introduced to the catalyst bed for 2 h with a flow of 50 ml min^{-1} at 700 °C and ambient pressure. While the catalyst reduction was conducted, the first reactor was heated at 600 °C. Next, water was added to the system with a flow of 1 ml min^{-1} until the pressure in the first part of the system reached its desired value of 265 bar. After this step, the liquid feed was introduced to the system with a volumetric flow rate of 1.6 ml min^{-1}. The EtOH concentration in the feed varied between 5 wt% and 20 wt%. The temperature and pressure of reactor I were set at 600 °C and 265 bar in all experiments. The mean residence time in this reactor was 1.5 min (calculated at experimental conditions), with deviations from this value due to the change in EtOH concentration being very small (standard deviation was 0.025 min). The temperature of the reactor II ranged from

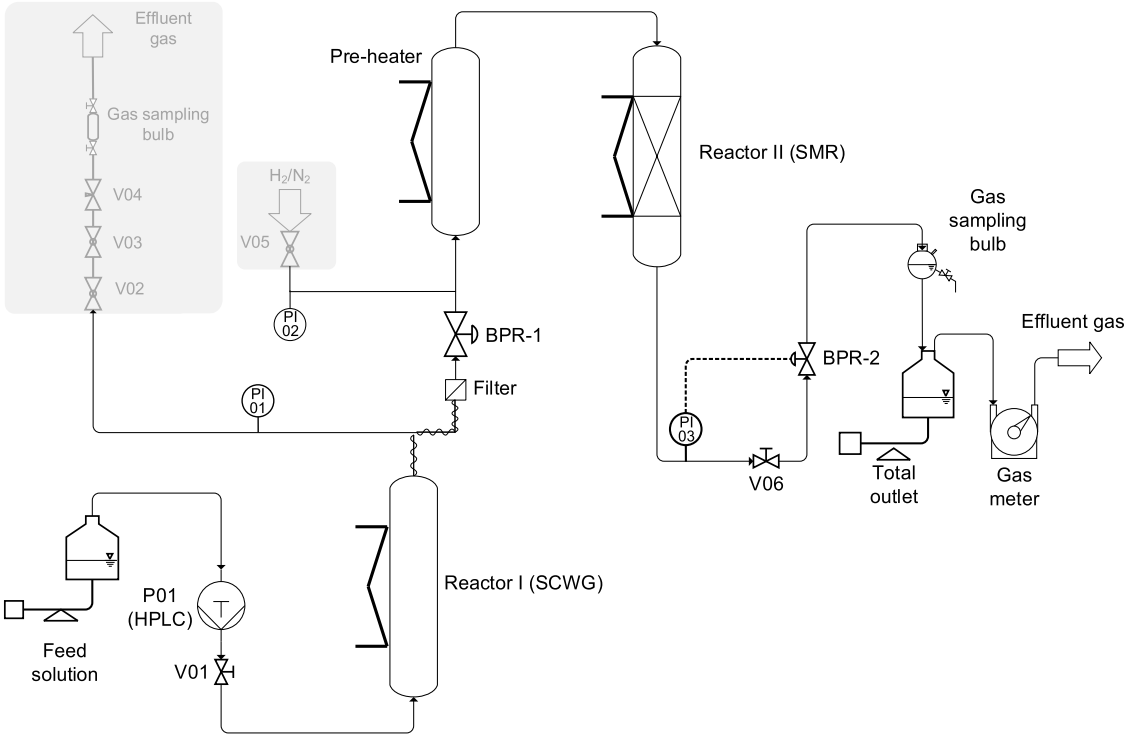

Fig. 1. Experimental layout. The auxiliary parts of the equipment are highlighted in grey. BPR: Back-pressure regulator.

700 °C to 800 °C and its pressure from 1 bar to 40 bar.

Gas samples were taken for analysis every half hour in a Gas Chromatograph (Hewlett-Packard Series II 5890 Plus model) equipped with a thermal conductivity and flame ionisation detectors and a silica capillary column (Carboxen 1010 PLOT 30 m, SUPELCO). Samples from the feed and from the liquid effluent are analyzed in a DIMATOC 2100 (DIMATEC), so that the total organic carbon (TOC) content of both can be determined.

For investigating the effect of operating conditions in the SMR reactor (temperature, pressure, and space velocity) and for the comparison between the two reforming catalysts the feed to the system was an EtOH/water solution with 8 wt% EtOH. For those experiments the SCWG of EtOH was non-catalytic, i.e., neither heterogeneous nor homogeneous catalyst was used.

The effect of the EtOH concentration on the product gas was explored, using five different concentrations from 5 wt% to 20 wt%. For this final set of experiments, in order to be sure that the system would operate with high gasification efficiency even under high EtOH concentration, 100 ppm of potassium in the form of $KHCO_3$ salt was added to each feed solution, acting as a homogeneous catalyst. The differences in the gasification product, due to the $KHCO_3$ addition, are discussed in section 3.2. The mass and carbon balances were calculated in every experiment. The mass balances ranged from 99% to 102%, while the range of the carbon balances was 95–105%.

The experimental data are compared with the thermodynamic equilibrium. The equilibrium values were calculated with the Aspen HYSYS V14 software. There, an RGibbs reactor was selected for simulating the SR of the SCWG product gas at various temperatures and pressures. The property package that was chosen for the calculations was the PRSV, which uses the Peng-Robinson equation of state.

Technical problems, such as leaks and clogging, prevented the system from operating with increased pressure in the second reactor at the beginning of the experiment. Usually, the problems were solved during the experiment gradually and by first checking the operation of the second reactor under atmospheric pressure. The same problems also prevented the continuous overnight operation of the process, with no effective solution so far. For this reason, the time on stream (TOS) for all experiments was 4 h. For the experiments comparing the activity of the two catalysts under different pressures, each catalyst was first subjected to atmospheric pressure for 4 h and then to an elevated value again for 4 h.

The effect of the gas hourly space velocity (GHSV) on hydrocarbon conversion and SR product gas composition was studied by varying the catalyst mass in the SR reactor. The GHSV is the ratio of the volumetric flow rate of the SCWG product at ambient conditions to the volume of the catalyst [28]. For the calculation of the catalyst bed volume, the apparent densities of the catalysts were used. The apparent density of the R210 was equal to 0.915 g ml^{-1} and that of the R330 was 1.01 g ml^{-1}. The parameters used for the evaluation of the performance of the SCWG process are the Carbon Gasification Efficiency (CGE, eq. (6)) and the yield of product gases (eq. (2.2)):

$$CGE(\%) = \frac{n_{C\ in\ product\ gas}(mol)}{n_{C,feed}(mol)} \tag{6}$$

and the yield of product gases:

$$Y_i\left(\frac{mol}{mol_{ethanol}}\right) = \frac{n_i(mol)}{n_{ethanol\ in\ feed}(mol)}, i = H_2, CH_4, CO_2, CO\ and\ C_{2+} \tag{7}$$

The S/C ratio of the SCWG product was calculated via equation (8):

$$\frac{S}{C} = \frac{\dot{n}_{H_2O_{SCWG}}\left(\frac{mol}{h}\right)}{\dot{n}_{CH_{4,SCWG}} + \dot{n}_{CO_{2,SCWG}} + \dot{n}_{CO_{SCWG}} + 2 \bullet \dot{n}_{C_2H_{6,SCWG}} + 3 \bullet \dot{n}_{C_3H_{8,SCWG}}\left(\frac{mol}{h}\right)} \tag{8}$$

where, $\dot{n}_{H_2O_{SCWG}}$, $\dot{n}_{CH_{4,SCWG}}$, $\dot{n}_{CO_{2,SCWG}}$, $\dot{n}_{CO_{SCWG}}$, $\dot{n}_{C_2H_{6,SCWG}}$, and $\dot{n}_{C_3H_{8,SCWG}}$ are the molar flow rates of the products from the SCWG reactor.

In order to study the performance of the SMR catalyst the conversion of CH_4 (eq. (9)) and higher hydrocarbons (eq. (10)) were used.

$$CH_4\ conversion\ (\%) = \frac{n_{CH_{4,inlet}} - n_{CH_{4,outlet}}}{n_{CH_{4,inlet}}} \tag{9}$$

$$C_{2+}\ conversion\ (\%) = \frac{\dot{n}_{C_{2+},inlet} - \dot{n}_{C_{2+},outlet}}{\dot{n}_{C_{2+},inlet}} \quad (10)$$

In addition to those equations, one more was used to assess the H_2 yield (eq. (12)), according to the stoichiometric reaction of EtOH steam reforming (eq. (11)):

$$C_2H_5OH + 3H_2O \rightarrow 6H_2 + 2CO_2,\ \Delta H^{298K} = 173.5\frac{kJ}{mol} \quad (11)$$

$$Y_{H_2,SR}(\%) = \frac{\dot{n}_{H_2,total}\left(\frac{mol}{h}\right)}{6 \bullet \dot{n}_{Ethanol}\left(\frac{mol}{h}\right)} \quad (12)$$

2.3. Characterization of fresh and used catalysts

Inductively coupled plasma-optical emission spectrometry (ICP-OES) was used for determining the actual composition of the catalysts. Digestion of the catalysts for ICP-OES was carried out in a mixture of 6 ml conc. H_2O_2, 2 ml conc. HNO_3 and 4 ml conc. HCl. Microwave irradiation of 600 W was applied for 90 min. The solution was diluted to a volume of 25 ml before being measured in an Agilent 725 spectrometer with a plasma excitation of 49 MHz and 2 kW.

The Brunauer-Emmett-Teller (BET) surface area and porosity of both fresh and reduced catalyst samples were determined by N_2 physisorption at 77 K with an Autosorb-1 (Quantachrome) flow apparatus.

Powder diffractograms of the catalyst were acquired with a PANalytical X'Pert Pro diffractometer using Cu-K_α radiation and a Ni-filter. The data were recorded in a step size of 0.033° with 2θ ranging from 5 to 120°. The full width at half maximum (FWHM) of the 111 reflection of nickel (44.5°) was determined by peak fitting with Origin2019. The FWHM was used to estimate the domain size using the Scherrer equation and LaB_6 as reference.

For thermogravimetric analysis coupled with mass spectrometry (TGA-MS), about 40 mg of the sample were loaded into a small crucible. The sample was flushed with 80 ml min^{-1} of Ar containing 10% O_2 for approximately 8 h. Afterwards the sample was heated with 5 °C min^{-1} to 1100 °C in the same flow. The gas concentration was monitored with a Netzsch QMS 403 D Aëolos mass spectrometer. Background correction with an empty crucible was performed. The data were analyzed with Origin2019. For the measurements a Netzsch STA 449 F3 Jupiter was used.

The H_2 temperature programmed reduction (TPR) was carried out in an Altamira AMI-300 device. A sample of 0.0808 g of catalyst was placed in a U-shaped quartz reactor and first dried with Ar at 200 °C (flow 30 ml min^{-1}, temperature ramp 10 K min^{-1} then 15 min at 200 °C) followed by cooling down to room temperature under Ar (20 K min^{-1}). The temperature was raised afterwards from room temperature to 950 °C at a rate of 5 °C min^{-1} (950 °C held for 10 min), in a gas mixture containing 10% H_2/Ar (flow 30 ml min^{-1}).

3. Results and discussion

3.1. Characterization of fresh catalysts

Table 1 presents the determined composition of the two catalysts from the ICP-OES measurements. The Ni-content of the R210 is 13.2 wt % while that of R330 is 9.6 wt%. Another difference between the two samples is the content in K, which is higher in R210. The physicochemical properties of the two fresh catalysts are presented in Table 2. Both catalysts had very low surface area due to the low surface area of the support [36,37], with the R330 having almost double the surface area of the R210.

Fig. 2 presents the X-ray diffractograms of the fresh and reduced catalysts. The main support crystal phases of the R330 were $CaAl_4O_7$ and $CaAl_{12}O_9$, while the crystal phases of the R210 were the $CaAl_4O_7$ and the $K_{2.6}Al_{21.83}O_{33.9}$. Both fresh catalysts consisted of NiO, which was sufficiently reduced to Ni^0, as the profiles of the reduced samples show. Traces of $NiAl_2O_4$ could be present since the TPR profile (Fig. 3) of both of them showed peaks at temperatures higher than 700 °C, but NiO and metallic Ni probably overlapped them. The sizes of the Ni crystallites in the reduced catalysts were calculated by the Scherrer equation to equal 40.3 nm for R330 and 35.8 nm for R210.

The TPR profile of the fresh NiO(14 wt%)/$CaAl_{12}O_9$ (R330) catalyst is given in Fig. 3, where it is shown that the main reduction peak centers at around 475 °C, followed by three shoulder peaks at 545 °C, 699 °C and 823 °C. The profile of the R210 catalyst is characterized by a main peak at 466 °C, a second one at 692 °C, and a third one at 782 °C. The peaks of the R210 were close to the ones of the R330 but shifted to slightly lower temperatures indicating the slightly enhanced reducibility of the R210. Both catalysts presented the most intense peaks at relatively low temperatures, which are ascribed to free NiO species closely connected with the support [38,39]. The last two peaks correspond to structures characterized by strong interaction between the Ni and the support and thus, are difficult to reduce, such as $NiAl_2O_4$ [39–43].

3.2. Assessing the product from the SCWG reactor

The investigation of the effect of temperature, pressure, and space velocity on the product gas from the second reactor (reformer) was carried out with an 8 wt% EtOH solution fed in the first reactor. Preliminary experiments addressed only the gasification in the first reactor, to determine its product. The average concentration of the dry product gas and the average yields of the products based on EtOH are given in Table 3. Hydrogen was the dominant component in terms of volumetric percentage, followed by CH_4. The average flow rate of the product gas was 13.4 NL h^{-1}, while the S/C ratio of the total product was 15.2. The average values of the carbon gasification efficiency (CGE) CGE and $Y_{H_2,SCWG}$ were 99.2% and 28.8%, respectively.

The effect of EtOH concentration (5–20 wt%) on the SCWG product composition was investigated first. In all tests the ethanol conversion was complete. Fig. 4 illustrates the composition of the dry product gas and how it varied with EtOH concentration. A decrease in H_2 concentration from around 52.5 vol% to 38.5 vol%, was observed when the EtOH concentration increased from 5 wt% to 20 wt%. The concentrations of CH_4 and C_{2+} hydrocarbons followed the opposite trend with gradual increase from 16 vol% to 24.6 vol%, and from 4.2 vol% to 8.7 vol%, respectively, while that of CO_2 showed a decrease from 26.9 vol% to 23.6 vol%. The hydrocarbons higher than CH_4 contain mostly C_2H_6. A notable upward shift in CO concentration was also observed, being more profound at higher EtOH concentrations than at lower ones, i.e., from 0.4 vol% at 5 wt% EtOH, it rose to 2.2 and 4.6 vol%, at 15 and 20 wt%, respectively.

The increase in C_{2+} hydrocarbons with the increase in EtOH concentration may result from the reaction of EtOH dehydration, forming

Table 1
Composition of the two catalysts employed for SR.

Catalyst	Ni content (wt. %)	K content (wt. %)	Ca content (wt. %)	Al content (wt. %)
R210	13.2	1.5	8.8	30.7
R330	9.6	0.2	9.5	30.8

Table 2
Physicochemical properties of the fresh catalysts.

Catalyst	BET surface area (m^2 g^{-1})	Pore volume (cm^3 g^{-1})	Pore diameter (nm)
R210	3.8	0.025	9.2
R330	7.4	0.028	6.7

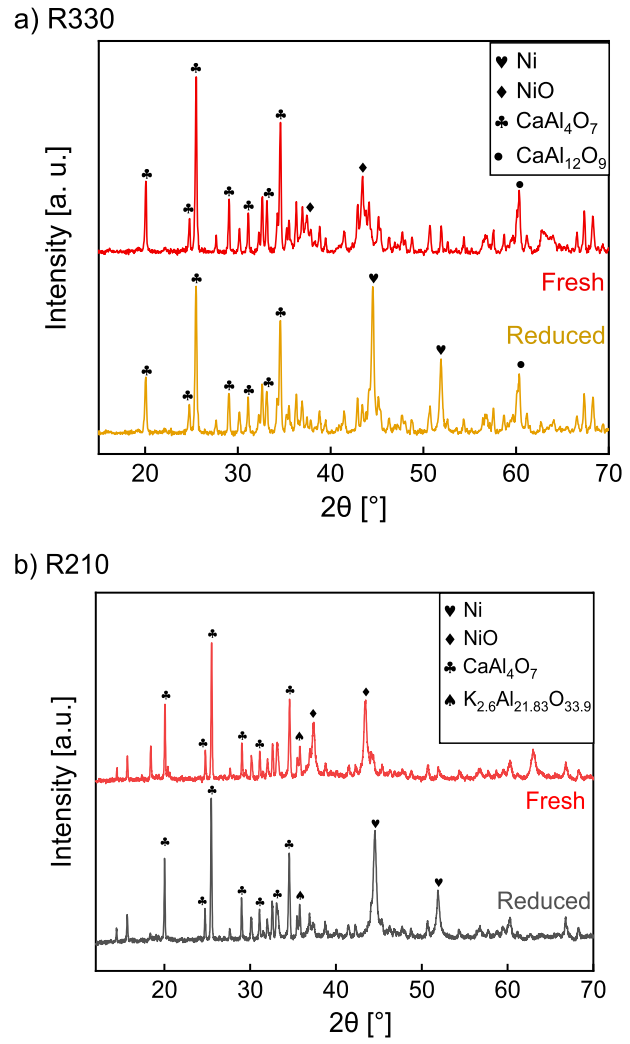

Fig. 2. a) XRD graphs of the fresh and reduced R330 and b) R210 catalysts.

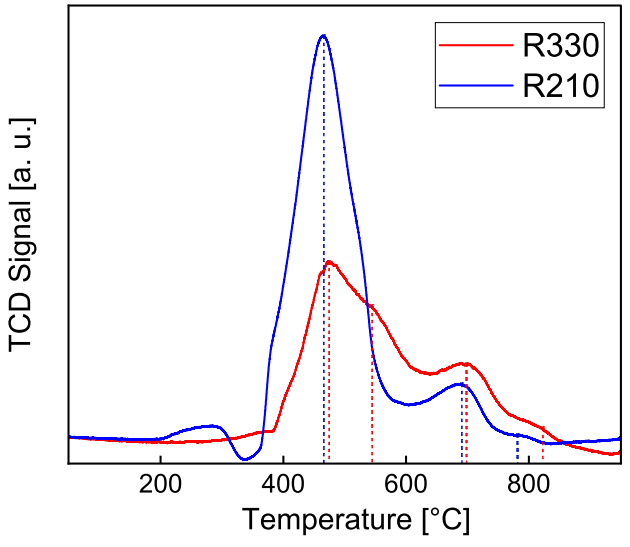

Fig. 3. H_2-TPR profile of the fresh catalysts.

Table 3
Concentrations and yield of the product gas species from 8 wt% EtOH SCWG at 600 °C and 265 bar.

Product gas	Dry gas composition [vol%]	Products' yield [mol mol_{EtOH}^{-1}]
H_2	48.6	1.7
CO	10.6	0.4
CH_4	22.7	0.8
CO_2	14.6	0.5
C_{2+}	3.7	0.1

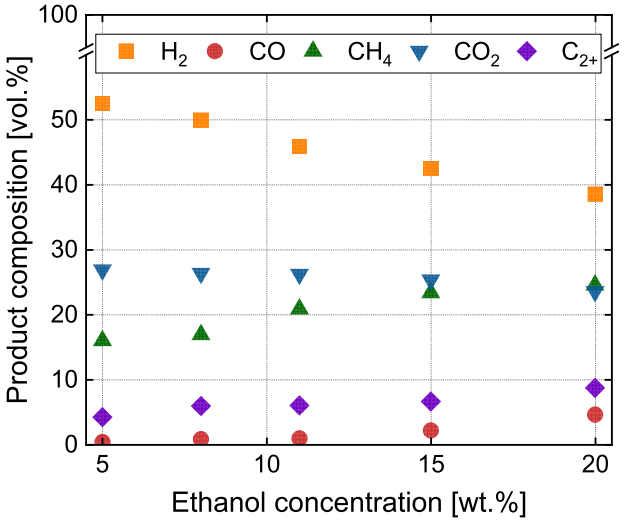

Fig. 4. Composition of the dry SCWG-product gas with concentration of EtOH in the inlet to the SCWG reactor.

ethylene (eq. (13)), which reacts subsequently with a H_2 molecule to form ethane (eq. (14)) [44,45]:

$$C_2H_5OH \rightarrow C_2H_4 + H_2O, \Delta H^\circ = 45.8 \frac{kJ}{mol} \quad (13)$$

$$C_2H_4 + H_2 \leftrightarrow C_2H_6, \Delta H^\circ = -136.3 \frac{kJ}{mol} \quad (14)$$

By comparing the concentration of CO in Table 3 and Fig. 4, for 8 wt % EtOH a significant drop in its concentration can be observed owing to the addition of $KHCO_3$. It has been reported by several studies that potassium can act as a catalyst, increasing gasification efficiency, promoting the WGS reaction and minimizing coke formation [46–50].

Table 4 presents the S/C ratio, the CGE, the amount of gas produced, and the $Y_{H_2,SCWG}$ of the SCWG product at different EtOH concentrations. The CGE was ≥97%, indicating almost complete gasification of EtOH, even at high organic feed concentrations. The factors that led to high CGEs, were the applied temperature of 600 °C [18], the long residence time of 1.5 min [51,52], and the addition of K^+. The S/C ratio as expected decreases drastically with increasing EtOH concentration. This parameter is very important for the operation of the SMR reactor, as it plays an important role in the conversion of hydrocarbons and the

Table 4
Main features of EtOH SCWG for different feed concentrations.

EtOH concentration (wt. %)	S/C ratio (mol_{H2O} mol_C^{-1})	Amount of product gas (L g_{EtOH}^{-1})	$Y_{H_2,SCWG}$ (mol mol_{EtOH}^{-1})	CGE (%)
5	22.0	2.02	0.37	99.6
8	12.9	1.90	0.32	99.6
11	7.8	1.94	0.31	99.4
15	6.3	1.62	0.24	97.9
20	4.5	1.48	0.20	97.0

hydrogen yield. This is because of the effect on the equilibrium of the SMR and WGS reactions [53], but also on formation of coke [54]. It has been reported that in steam reforming of CH_4 and other hydrocarbons, or mixtures thereof, there are critical S/C ratios, at given temperature and pressure, above which the carbon formation is inhibited [55,56]. Generally, with an increase in the carbon content, the S/C ratio should also increase to avoid the formation and deposition of carbon on the catalyst [12]. As the EtOH concentration increases, the amount of steam decreases while the amount of carbonate species increases. Therefore, after a certain concentration of EtOH, the remaining steam will not be enough to prevent carbon formation and deposition. Additionally, the $Y_{H_2,SCWG}$ decreases with EtOH concentration as does the percentage of hydrogen in the dry product gas.

3.3. Effect of temperature and pressure on the products of the steam reformer

To study the effect of temperature and pressure on the conversion of CH_4 and the composition of the product gas in the steam reformer, an 8 wt% EtOH solution was used as feed to the SCWG reactor and the catalyst in the steam reformer was the R330. Fig. S1 in the Supporting Information depicts the conversion of CH_4 with temperature and pressure at thermodynamic equilibrium, and Fig. S2 shows the respective dry product gas composition. From Fig. S1, it is evident that increasing temperature has a positive effect on CH_4 conversion, whereas increasing pressure has a negative effect. More specifically, under thermodynamic equilibrium, CH_4 conversion drops from almost 100%–86% at 700 °C when the pressure increases from 1 to 40 bar. At 750 °C, the corresponding CH_4 conversion at 40 bar is 94.6%. Similarly, the concentration of hydrogen produced at equilibrium falls from 75.5 vol% at 700 °C and 1 bar to 74 vol% at 700 °C and 40 bar. At 750 °C, the concentration of H_2 at equilibrium ranges from 75.4 vol% at 1 bar to 74.9 vol% at 40 bar. The CH_4 concentration was found to increase with pressure and decrease with temperature. At atmospheric pressure, CH_4 levels remained close to zero across all temperatures tested. Under conditions of 700 °C and 40 bar, the CH_4 concentration reached 1.6 vol%, whereas at 750 °C and the same pressure, it only reached 0.6 vol%. Additionally, an increase in temperature resulted in a slight rise in CO concentration: at 700 °C and 30 bar, CO was at 2.6 vol%, while at 750 °C and 30 bar, it increased to 3.3 vol%. Conversely, increasing pressure had a minor negative impact on CO levels. In contrast, CO_2 concentration was higher at lower temperatures, due to the WGS reaction [30]. Specifically, at 700 °C and 40 bar, CO_2 concentration was 21.8 vol%, which dropped to 21.3 vol% at 750 °C under the same pressure. Overall, within the studied range of pressures and temperatures for the product gas from 8 wt% EtOH in SCWG (at 600 °C and 265 bar), the effect of temperature and pressure on CH_4, H_2, CO, and CO_2 concentrations remains relatively minor.

Fig. 5 depicts the experimental CH_4 conversion as a function of pressure in the second reactor, for different temperatures. By comparing the results from Fig. 5 to those in Fig. S1, a close agreement between the experimental results and the equilibrium values can be observed at pressures close to 1 bar, where CH_4 conversion is almost complete. As pressure increases, the deviation from thermodynamic equilibrium also

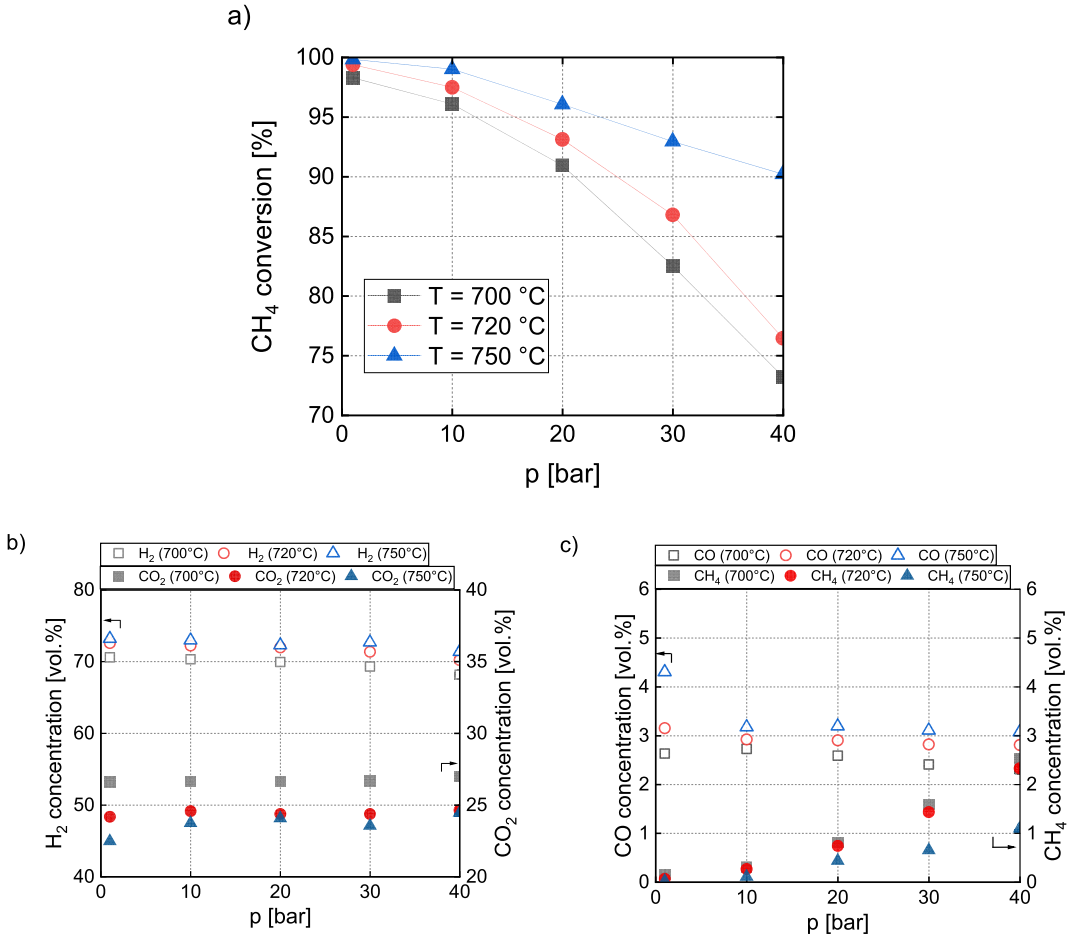

Fig. 5. a) Conversion of CH_4 versus pressure for different temperatures in the SR reactor, b) Concentration of H_2 and CO_2 in the SR dry product gas versus pressure for different temperatures in the SR, and c) Concentration of CH_4 and CO respectively (SCWG with 8 wt% EtOH at 600 °C and 265 bar; GHSV in SR reactor = 63500 h^{-1}).

increases. However, increasing temperature counteracts this deviation, reducing it. At 700 and 720 °C, the difference between the experimental results and equilibrium values is already significant at 20 bar. For example, the experimental CH_4 conversion at 720 °C and 20 bar was 93%, while the equilibrium value was 97%. This is not the case at 750 °C, where the largest difference between the experiments and equilibrium occurs at 40 bar, with the experimental CH_4 conversion at 90%, compared to the equilibrium value of 94.6%.

The variations in product composition with pressure and temperature are rather minimal in agreement with thermodynamic equilibrium. Regarding the experimental results for the concentration of CH_4 (Fig. 5c), it decreased with temperature and increased with pressure. At 700 °C, the CH_4 content in the dry product gas amounted for 0.2 vol% at 1 bar, whereas at 750 °C it reduced to 0.02 vol%. Likewise, at 40 bar and 700 °C its value was equal to 2.5 vol%, but dropped eventually to 1.1 vol % at 750 °C. At equilibrium, the CH_4 concentration ranges from 0.001 vol% at 1 bar, to 1.7 vol% at 40 bar, under 700 °C, but at 750 °C, its concentration is $4 \bullet 10^{-4}$ vol% at 1 bar, and 0.6 vol% at 750 °C.

These experimental findings demonstrate the profound effect of temperature and pressure on the reactions of SMR and WGS. The temperature increase promotes the forward SMR reaction and the reverse WGS, thereby increasing the percentage of H_2 and CO, and the methane conversion [57,58]. Increasing pressure favors the reverse SMR reaction, decreasing CH_4 conversion and the concentrations of H_2 and CO [59], but it does not affect the WGS reaction, leaving the residual steam to react with CO, forwarding the slight increase in CO_2 [28,60].

Temperatures higher than 750 °C were tested but rapid deactivation of the R330 catalyst was observed. BET analysis indicated a surface area loss from 7.4 $m^2\ g^{-1}$ to 1.7 $m^2\ g^{-1}$, a pore volume loss from 0.028 to 0.014 $cm^3\ g^{-1}$ and a pore diameter shrinkage from 6.7 to 1.7 nm. Most likely the catalyst pores have been blocked during the reaction under T > 750 °C. The XRD diffraction profile of the catalysts subjected to 770 °C is given in Supporting Information (S2). All peaks that were found in the freshly reduced catalyst, related to the support, were found here too. No NiO peaks were found, only metallic Ni, with a crystallite size of 45.7 nm, calculated by the Scherrer equation. However, as will be seen in the following sections (3.5 and 3.6), sintering was comparable to values of other samples that did not show dramatic deactivation. No carbon was found on the used catalyst via TGA-MS (see S2). A possible reason for deactivation might be the collapse of the porous structure of the support [61,62].

3.4. Effect of space velocity on the SR product

The effect of the GHSV and its effect on the product gas from the reformer was also studied. The temperature of the catalytic bed was 730 °C and measurements were performed for two different pressures (1 and 30 bar). The results regarding CH_4 conversion are summarized in Fig. 6a. The GHSV spans from 42400 h^{-1} to 127000 h^{-1}. Under a pressure of 1 bar, the deviation from the thermodynamic equilibrium (CH_4 conversion almost 100%) is negligible for GHSVs, up to 63500 h^{-1}. As the GHSV increases to 127000 h^{-1}, the CH_4 conversion under atmospheric pressure deviates significantly from equilibrium as it falls to 84.1%. At a pressure of 30 bar, the deviation of the equilibrium is already apparent at a GHSV of 50900 h^{-1}, where it falls to 89.3%, while the equilibrium value is around 94%. The highest GHSV of 127000 h^{-1} resulted in a CH_4 conversion equal to 75%. However, a GHSV of 42400 h^{-1} was enough for the CH_4 conversion to reach close to equilibrium and be equal to 93.7%.

Fig. 6b and 6c depict the dry product gas composition as a function of GHSV at 730 °C and for 1 and 30 bar. The percentage of H_2 at 1 bar falls from 72.6 vol% to 70.8 vol%, from 42400 h^{-1} to 127000 h^{-1}. Its percentage is also reduced at 30 bar, from 71.4 vol% to 69.4 vol%, under 42400 h^{-1} and 127000 h^{-1}, respectively. The percentage of CO_2 was

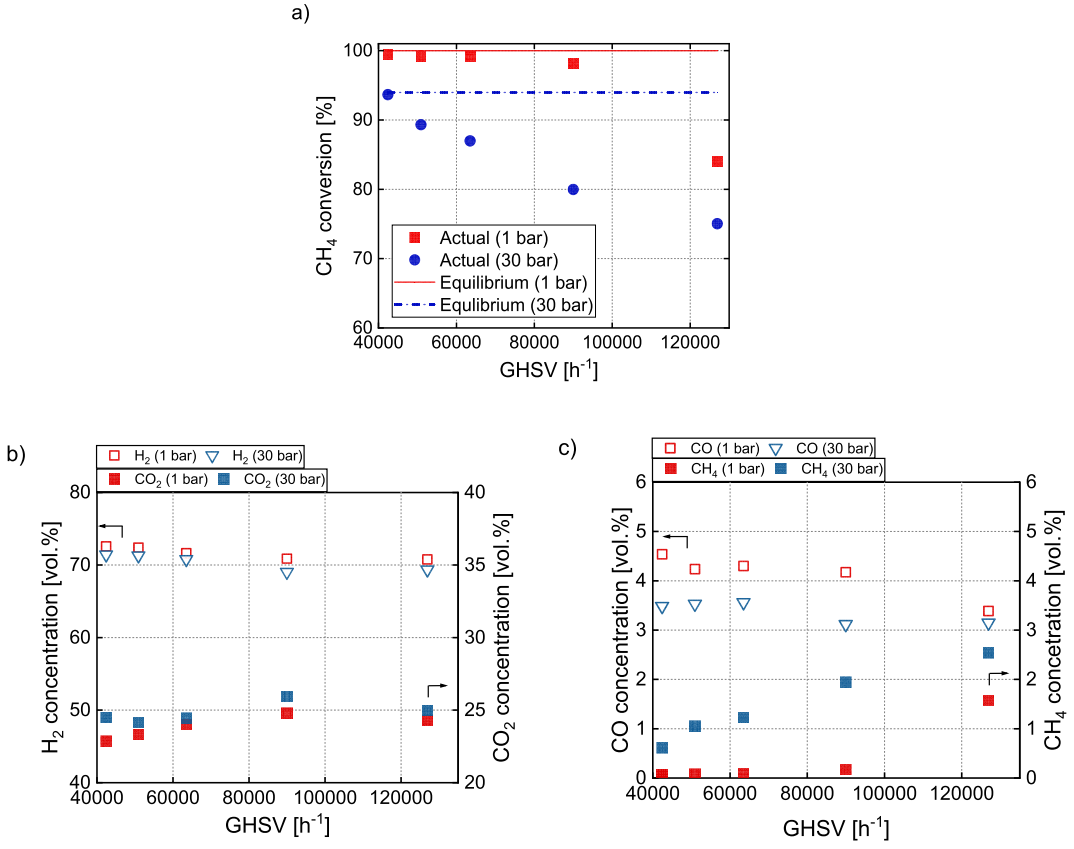

Fig. 6. a) Conversion of CH_4 with GHSV for different pressures in the SR reactor, b) Concentration of H_2 and CO_2 in the SR dry product gas with GHSV for different pressures in the SR reactor, c) Concentration of CH_4 and CO respectively (SCWG with 8 wt% EtOH at 600 °C and 265 bar; T in the SR reactor = 730 °C).

slightly increased with increasing GHSV, from 22.9 vol% to 24.3 vol%, at 1 bar, and from 24.5 vol% to 25.0 vol% at 30 bar. In Fig. 6b an increase in CH_4 concentration is observed at both pressures, i.e., from 0.05 vol% to 1.6 vol% at 1 bar, and from 0.6 vol% to 2.5 vol% at 30 bar. Last, the concentration of CO follows a downward trend with rising GHSV, from 4.5 vol% to 3.4 vol%, and from 3.5 vol% to 3.1 vol%, at 1 bar and 30 bar respectively. No hydrocarbons higher than CH_4 were observed in the SR product gas.

3.5. Effect of EtOH concentration on the SR product and on the catalyst

The concentration of EtOH in the SCWG reactor varied from 5 wt% to 20 wt%. The effect of ethanol concentration on the product distribution exiting the supercritical gasifier was already presented in 3.2. Fig. 4 demonstrates the change in the outlet dry product gas composition from the SCWG reactor. Table 4 indicates how the S/C ratio, the hydrogen yield, and the amount of the SCWG product gas vary with the concentration of organic feedstock. This section investigated the effect of the EtOH concentration on the reformate product gas. The SR reactor operated at 730 °C, 30 bar, with a constant catalyst mass of 2.5 g. The catalyst used was the R330, i.e., the NiO(14 wt%)/$CaAl_{12}O_9$. Due to changes in the volumetric flow of the product gas with varying EtOH, the GHSV varied accordingly. However, the differences in GHSV were minimal, with the mean value and the standard deviation being equal to 47877 h^{-1} and 2134 h^{-1}, respectively. This GHSV value is near the one reported in the previous section (section 3.4, Fig. 6), i.e., 42400 h^{-1}, which was sufficient to drive the reactions in the SR reactor close to thermodynamic equilibrium.

The CH_4 conversion and the total H_2 yield after SCWG and subsequent SR for different EtOH concentrations are given in Fig. 7a. Fig. 7b depicts the respective SR product gas composition. The CH_4 conversion falls from 97.5% with 5 wt% EtOH to 22.5% with 20 wt% EtOH. Likewise, the H_2 yield falls from 98.6% to 58.3%, as the EtOH concentration increases from 5 wt% to 20 wt%. The volumetric percentages of H_2 and CO_2 in the SR product gas follow a decreasing trend with EtOH concentration increase, with the first dropping from 72.0 vol% to 62.3 vol%, and the second from 25.8 vol% to 21.8 vol%, from 5 wt% to 20 wt% EtOH, respectively. On the other hand, in this EtOH concentration range, the concentration of CH_4 and CO increase, i.e., methane increases from 0.2 vol% to 9.5 vol%, and carbon monoxide from 2.1 vol% to 6.5 vol%. It is worth noting that there were no C_{2+} hydrocarbons in the SR product, even at high EtOH concentrations. Section S4 in the Supplementary Material includes the corresponding results at thermodynamic equilibrium. The differences between the experimental values and those at thermodynamic equilibrium are relatively minor, with the experimental results following the same trend as the equilibrium values in terms of CH_4 conversion, H_2 yield, and product gas composition. The deviation from equilibrium in CH_4 conversion becomes more significant at high EtOH concentrations. For example, at 20 wt% EtOH, the equilibrium CH_4 conversion was 36%, while the experimental value was 22.5%.

According to the results from Fig. 4 and Table 4, the increase in EtOH concentration results in an SCWG product gas with a higher CH_4, C_{2+}, and CO content and a significantly lower S/C ratio. At high EtOH concentrations, the consumption of steam for the SR of the C_{2+} hydrocarbons further decrease the available steam for SR of CH_4. The increase in these components and the simultaneous decrease in the steam content in the gas fed to the SR reactor drive the equilibrium of the SMR reaction towards lower CH_4 conversion [27,63,64] and the equilibrium of the WGS reaction towards CO production [27].

The Weisz-Prater criterion was calculated to assess mass transfer limitations within the catalyst pores of the steam reforming reactor [65], under varying EtOH concentrations in the SCWG reactor. A description of this criterion, along with a detailed calculation methodology and corresponding values at different EtOH concentrations, is provided in the Supplementary Material (S5, Table S3). At an EtOH concentration of

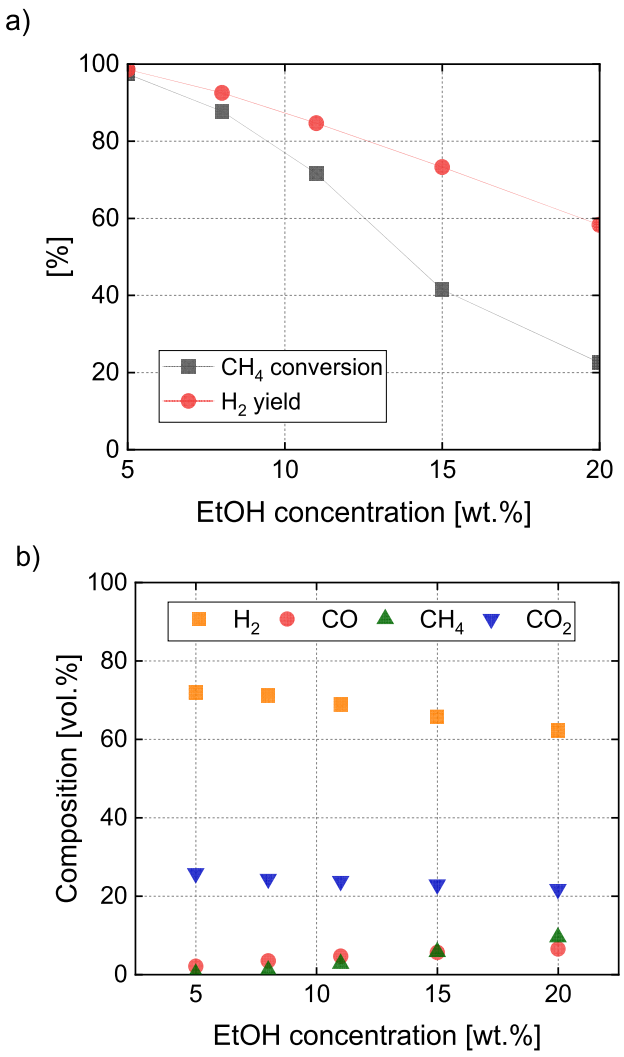

Fig. 7. a) Conversion of CH_4 and H_2 yield after SR with different EtOH concentrations in the SCWG reactor and b) SR product gas composition with different EtOH concentrations in the SCWG reactor (SCWG at 600 °C and 265 bar; T in the SR reactor = 730 °C; p in the SR reactor = 30 bar; the catalyst mass was constant at 2.5 g and the mean GHSV value was 47877 h^{-1}).

5 wt%m the value of the criterion was 1.7 ≫ 1, indicating that diffusion within the catalyst pores limits the chemical reactions of steam methane reforming. As the EtOH concentration increased, the criterion value decreased substantially, reaching 0.0138 at 20 wt%, which highlights the absence of intra-particle diffusional limitations at higher EtOH concentrations. This trend correlates with the increasing amount of hydrocarbons, particularly CH_4, in the feed to the second reactor as EtOH concentration rises, resulting in higher CH_4 partial pressure and a lower S/C ratio in the SR reactor feed. In a recent study [18], Pashchenko demonstrated that an increase in the S/C ratio during steam methane reforming reduces the effectiveness factor, which is the ratio of the reaction rate with diffusion limitations to the reaction rate without these limitations. Pashchenko attributed this to the decrease in CH_4 partial pressure, which reduces methane diffusion more rapidly than the reaction rate.

The S/C ratio dropped from 22.0 to 4.5, when the EtOH concentration increased from 5 wt% to 20 wt%. An additional aim of this study was to investigate if this significant change in the S/C ratio would affect the catalyst structure. For this, two experiments were carried out, one with 5 wt% EtOH and one with 20 wt%. This time, however, the amount of catalyst was adjusted so that the parameter $m_{cat.}/\dot{F}_{HCs}$, with $\dot{F}_{HCs}$ being

the molar flow of the hydrocarbons generated in the SCWG reactor, to be the same in both cases and equal to its value when the EtOH concentration was 8 wt% and the catalyst mass was 2.5 g. The adjusted catalyst mass was thus 1.5 g at 5 wt% EtOH and 7.0 g at 20 wt% EtOH.

$$\left[\frac{m_{cat.}}{\dot{F}_{HCs}}\right]_{5\ wt.\%} = \left[\frac{m_{cat.}}{\dot{F}_{HCs}}\right]_{20\ wt.\%} = \left[\frac{m_{cat.}}{\dot{F}_{HCs}}\right]_{8\ wt.\%} = 16.7\ \frac{g_{cat.} \bullet h}{mol_{HCs}}$$

The overall GHSV under 5 wt% EtOH was now 84405 h^{-1}, and 17017 h^{-1} under 20 wt% EtOH. Fig. 8 presents the resulting CH_4 conversion, H_2 yield, and the dry product gas composition for these two cases. The conversion of CH_4, in the case of 5 wt% EtOH, was 93.8%, while its respective value under equilibrium is 98.6%. Similarly, for the case of 20 wt% EtOH, the experimental value of the CH_4 conversion was 32.0% and its equilibrium value is 36.0%. The respective product gas compositions were close with their equilibrium values. Therefore, although there is a difference in the overall GHSV between these two cases, both deviate roughly the same from their individual equilibrium. Their main difference still lies in the composition of the feed, i.e., S/C ratio and dry gas composition.

Fig. 9 presents the TGA profiles and the corresponding MS profiles of the catalysts exposed to the SR of product gas derived from 5 wt% and 20 wt% EtOH and also the reduced catalyst prior to reaction. The catalyst subjected to the lower EtOH concentration exhibited a slight mass loss, reaching 98.8% in the temperature range of 100–340 °C, likely due to water vaporization, as indicated by Fig. 9b. Subsequently, its weight increased to 101.1%, possibly due to the reoxidation of Ni. The small CO_2 peak observed around 635 °C corresponded to a negligible weight decrease from 101.10% to 101.08%. The catalyst subjected to the higher EtOH concentration showed a more significant weight loss at approximately 95.8% in the same temperature range of 100–340 °C. This was followed by a 1.32% weight increase possibly due to the reoxidation of Ni. On the contrary, the catalyst subjected at lower EtOH concentration had a weight gain of 2.3%, due to Ni reoxidation, aligned with the reduced catalyst sample. The reason for the lower weight increase might be ascribed to catalyst reoxidation under reaction conditions. A subsequent weight decrease, down to 95.7%, was observed between 600 °C and 800 °C. As shown in Fig. 9c, a CO_2 peak at 660 °C indicated part of this weight loss was due to the oxidation of filamentous carbon deposited on the catalyst [66]. However, this did not cause deactivation during the 4-h operation.

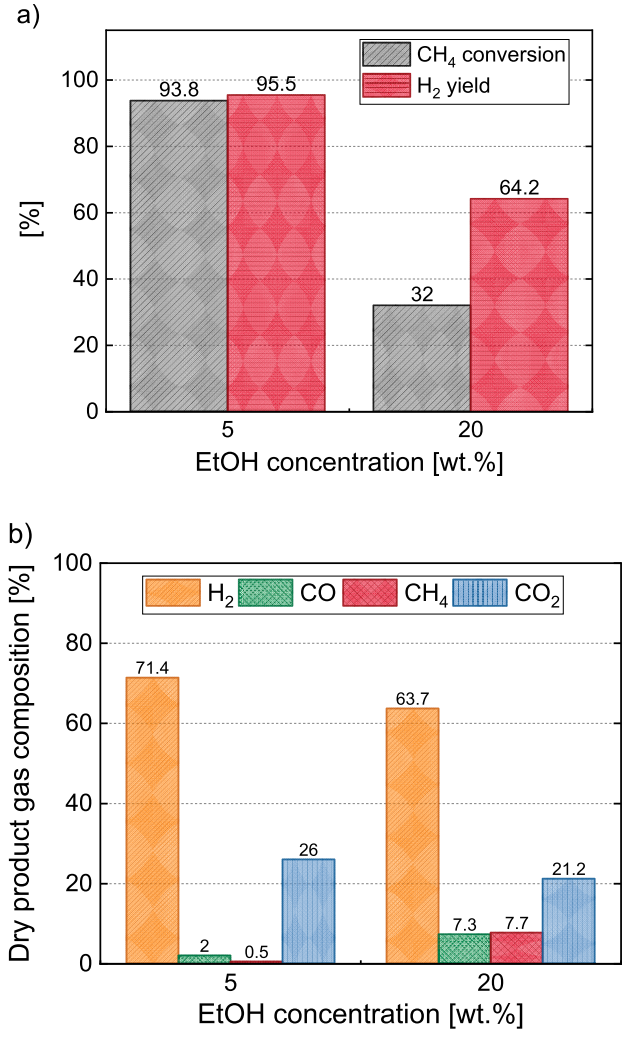

Fig. 8. a) Conversion of CH_4 and H_2 yield and b) Dry product gas composition, after SCWG-SR with 5 wt% and 20 wt% EtOH (SCWG at 600 °C and 265 bar; T in the SR reactor = 730 °C; p in the SR reactor = 30 bar; $m_{cat.}/\dot{F}_{HCs}$ = 16.7 $g_{cat.}$ h mol_{HCs}^{-1}).

The relatively low formation of carbon in both the 5 wt% and 20 wt% EtOH cases can be attributed to the excess steam, which suppresses carbon formation and deposition [54–56]. Additionally, the presence of H_2 in the feedstock for the SR reactor has been shown to inhibit carbon formation [55,67]. Furthermore, the basicity of the Ca–Al support contributes to reduced carbon formation [68,69].

Fig. 10 illustrates the XRD profiles of the used catalysts under SR following the SCWG of 5 wt% and 20 wt% EtOH. Both used catalysts demonstrated the same support structure with the reduced catalyst prior to the reaction (see Fig. 2). The dominant phase for the Ni species in the bulk catalyst was still the monometallic Ni, indicating that the H_2 produced in the SCWG reactor maintained the reduced state of Ni in both cases [28,70]. The catalyst subjected to the product gas from 20 wt% EtOH SCWG had a Ni crystallite size of 41.7 nm, whereas the one from 5 wt% EtOH SCWG had a Ni crystallite size of 40.9 nm. The difference in the Ni sizes between the two experiments is very small and both are close to the size of the reduced catalyst (40.3 nm). Therefore, sintering did not play a role in catalyst activity and overall process performance, for a TOS of 4 h. Long-term experiments are required in both cases in order to study the evolution of sintering.

The differences in the dry product gas composition and S/C ratio under the studied EtOH concentration range (5–20 wt%) seemed to have not affected the catalyst structure. Christensen et al. [71] performed sintering experiments on a commercial Ni/$CaAl_2O_4$ with a BET surface area of 5.5 m^2 $g_{cat.}^{-1}$. They argued that a significant change in the particle size or the surface area of this catalyst was difficult, since it already had a very small initial surface area, hindering, thus, the diffusion of Ni on it.

3.6. Comparison of the two catalysts

The catalysts R330 and R210 were tested under different pressures, constant temperature of 740 °C, constant catalyst mass of 2 g, so that the parameter $m_{cat.}/\dot{F}_{HCs}$ was equal to 12.5 $g_{cat.}$ h mol_{HCs}^{-1} for both catalysts, and a TOS of 8 h. The SCWG conditions were 600 °C and 265 bar, with the EtOH concentration in the feed being 8 wt%. Fig. 11a, 11.b, and 11 (c) depict the conversion of CH_4 and the SR product gas composition for the two catalysts, respectively. The CH_4 conversion of R330 was slightly higher than that of R210 for pressures in the range 1–10 bar. Specifically, the CH_4 conversion for the R330 was 98.3% and 96.5%, under 1 bar and 10 bar, respectively, whereas, the conversion for R210 was 96.8% and 94.5%. However, for pressures higher than 20 bar the CH_4 conversion of the R330 had a sharper decrease and fell to lower values than the R210, e.g., the conversion of the R330 at 40 bar was 74.3%, while that of the R210 was 84.1%. Similarly, it can be seen in Fig. 11b that, under a pressure in the range 1–10 bar, the concentration of CH_4 for the R330 was 0.2–0.3 vol%, while for the R210 it was 0.3–0.6 vol%. However, the pressure increase led to higher final CH_4 concentrations for R330 than R210, e.g., at 40 bar, the CH_4 concentration was 2.4 vol%

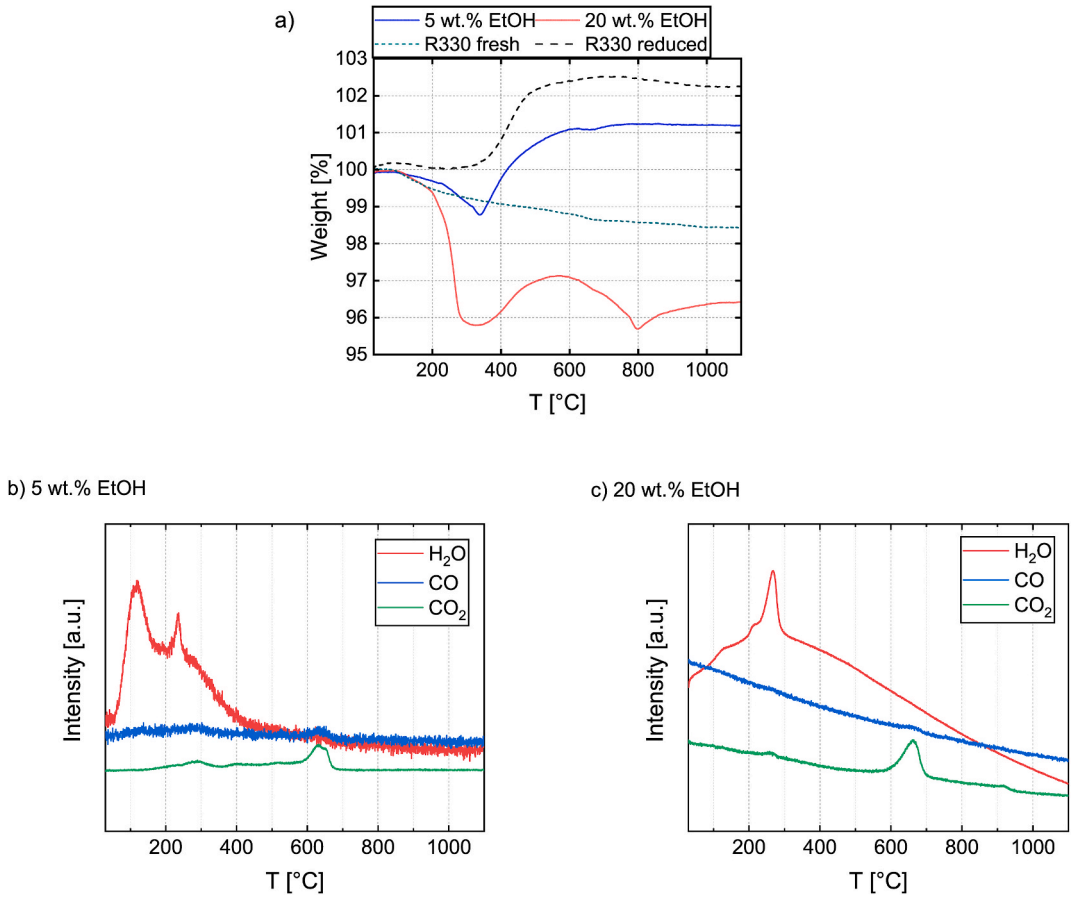

Fig. 9. a) TGA of the fresh, reduced, and used catalyst samples that were subjected at SR of the product gas from 5 to 20 wt% EtOH SCWG, b) MS signals of water vapor and carbon oxides of the used catalyst sample that was subjected at SR of the product gas from 5 wt% EtOH SCWG and c) MS signals of water vapor and carbon oxides of the used catalyst sample that was subjected at SR of the product gas from 20 wt% EtOH SCWG.

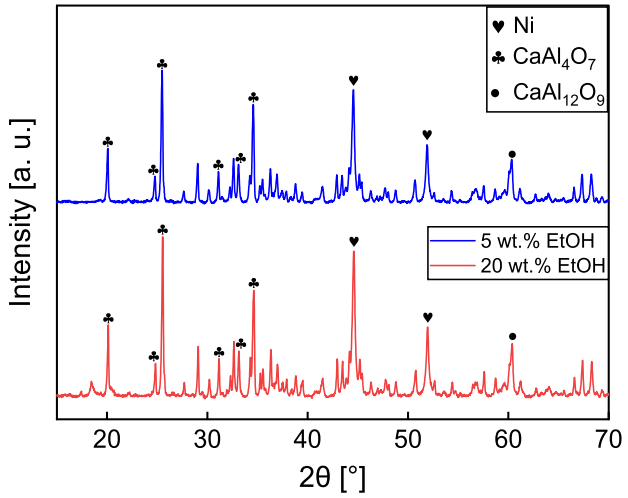

Fig. 10. XRD profiles of the used catalysts under SCWG and SR with 5 wt% and 20 wt% EtOH. SCWG at 600 °C and 265 bar; T in the SR reactor = 730 °C; p in the SR reactor = 30 bar; $m_{cat.}/\dot{F}_{HCs} = 16.7\ g_{cat.}\ h\ mol_{HCs}^{-1}$.

for R330 and 1.6 vol% for R210.

It was examined whether this difference in the activity of the two catalysts between low and high pressures could be attributed to the external and/or internal mass transfer control. For external diffusion control, the Mears criterion was applied [72].

$$M = \frac{r_A \bullet \rho_b \bullet R \bullet n}{k_c \bullet C_{A(bulk)}} \ll 0.15 \tag{15}$$

where r_A is the reaction rate of the limiting reactant in mol $kg_{cat.}^{-1}\ s^{-1}$, ρ_b is the apparent density of the catalyst in kg m^{-3}, R is the radius of the catalyst particles in m, n the reaction order, k_c the gas-particle mass transfer coefficient in m s^{-1}, and $C_{A(bulk)}$ the concentration of the limiting reactant in the bulk gas phase in mol m^{-3}. The Weisz-Prater criterion was applied for internal diffusion control [65].

$$WP = \frac{r_A \bullet \rho_c \bullet R^2}{D_{eff.} \bullet C_{A(surface)}} \ll 1 \tag{16}$$

where ρ_c is the actual density of the catalyst in kg m^{-3}, $D_{eff.}$ the effective diffusivity in $m^2\ s^{-1}$, and $C_{A(surface)}$ the concentration of the limiting reactant on the catalyst surface in mol m^{-3}.

The values of both criteria as well as the methods for calculating them for both catalysts are given in Supplementary Material (S5). The Mears criterion is satisfied, and therefore, the effect of external mass transfer is not considered as likely. On the other hand, at atmospheric pressure, the Weisz-Prater ratio receives values higher than unity. At pressures higher than 20 bar, the Weisz-Prater ratio falls two orders of magnitude lower than unity. Thus, under low pressures (1–10 bar), there is a strong resistance to the chemical reaction within the catalyst pores due to the intraparticle diffusion. Thus, the rather unexpected performance of the catalysts under low pressures (1–10 bar) can be ascribed to the intraparticle diffusion.

The resistance to the reaction due to intraparticle diffusion becomes insignificant under high pressures (p > 20 bar), where the R210

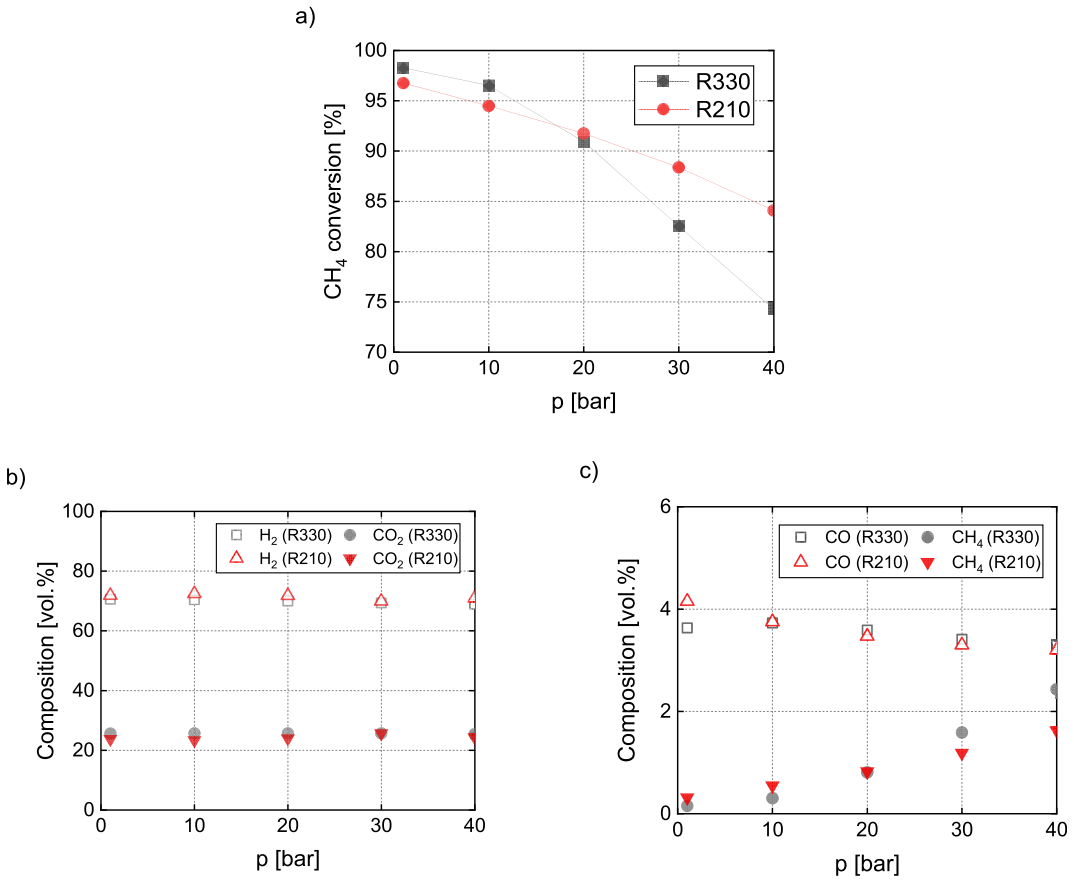

Fig. 11. a) CH_4 conversion for R330 and R210 after SR at 740 °C with a constant catalyst mass of 2 g, under varied pressure, b) respective concentration of H_2 and CO_2 for both catalysts in the SR products, and c) respective concentration of CO and CH_4 for both catalysts in the SR products (SCWG conditions: 600 °C, 265 bar, EtOH in the feed was 8 wt%).

dominated over the R330 in terms of CH_4 conversion. The higher activity in SR reaction of R210 compared to that of R330 could be attributed to its higher Ni content (13.2 wt% and 9.6 wt%, respectively) and the smaller initial Ni crystallite size (35.8 nm and 43.1 nm, respectively) [43,73,74]. However, as will be shown later with the XRD profiles of the used catalyst samples, the Ni crystallite sizes of both catalysts after the reaction were found to be nearly identical (59.2 nm and 60.0 nm), indicating that the dispersion does not play the primary role in the difference in activity, but rather the Ni loading. Apart from those two aspects that can similarly promote the WGS reaction, according to Garbarino et al. [75], the promotion of a commercial Ni-based catalyst with calcium aluminate as support with K_2O may hinder the reverse WGS at high temperatures, allowing the R210 to reach lower CO concentrations.

The catalysts exposed to 30 bar pressure were characterized using TGA-MS and XRD. Fig. 12a shows the TGA profiles, and Fig. 12b and 12c displays the corresponding MS profiles for the two catalysts. Both catalysts began to lose weight around 120 °C, attributed to water evaporation. This weight loss due to water release continued at approximately 200 °C and 278 °C, corresponding to the desorption of chemisorbed water [73]. Between 260 °C and 300 °C, both catalysts exhibited small peaks of CO_2 and CO, related to reactive carbon species [76]. At 400 °C, the weight of R210 decreased to 84.5%, while R330 reached 81.5%. Since the intensity of the water-related peaks was much higher than that of the carbon oxides, it can be implied that the primary cause of the weight loss is due to water desorption. R210 also showed a slight CO_2 release at around 340 °C. However, the overall weight loss for R330 was higher, suggesting that the carbon oxide peaks observed between 200 °C and 400 °C were of minor significance. Beyond 400 °C, a further weight decrease, likely due to water adsorbed in the inner layers of the catalyst, was observed. R210 showed a small CO_2 peak at 664 °C, resulting in a negligible weight loss of 0.3%. Similarly, R330 experienced a loss of 0.3% due to CO_2 release at a higher temperature (720 °C). In both cases, the CO_2 formation could be attributed to the oxidation of carbon filaments [66]. Additionally, both catalysts exhibited minor weight loss with small CO_2 peaks in the 890 °C–940 °C range, likely due to the oxidation of graphitic carbon [69,77]. R210 showed a decrease of 0.3%, and R330 a decrease of 0.5%.

The XRD profiles of R210 and R330 are given in Fig. 13. Both used catalysts depicted peaks at 44.5° and 51.8°, which resembled metallic Ni [78]. Unlike the R330, the R210 showed no peaks related to its support structure without however indicating signs of deactivation. The Ni particle sizes of the used catalysts were calculated by the Scherrer equation and were found to be almost similar. The Ni particle size of R210 was equal to 59.2 nm, accounting for a 65.4% increase compared to the initial size in the reduced state of the catalyst, while the respective one of R330 was 60 nm, and its relevant increase was 48.9%. It is thus apparent that the Ni crystallites on the R210 were more prone to sintering than the ones on the R330. Sehested et al. [61] showed that under 31 bar and a feed consisting of an H_2O:H_2 ratio of 10, the carrier's promotion with potassium accelerated the sintering of nickel crystallites compared to an unpromoted catalyst. The amorphization that the R210 underwent, without any loss in its activity, was also evident in our former publication, where the catalyst was also used for the SR (600 °C, 1 atm, GHSV = 44557 h^{-1}) of the SCWG product gas from 8 wt% EtOH gasification [28].

The loss in activity due to sintering could not be identified, because both samples were subjected at first to 1 bar and then, after 4 h, to 30 bar. Thus, any deactivation that would occur due to sintering was overlapped by the changes induced by the pressure increase. Longer TOS

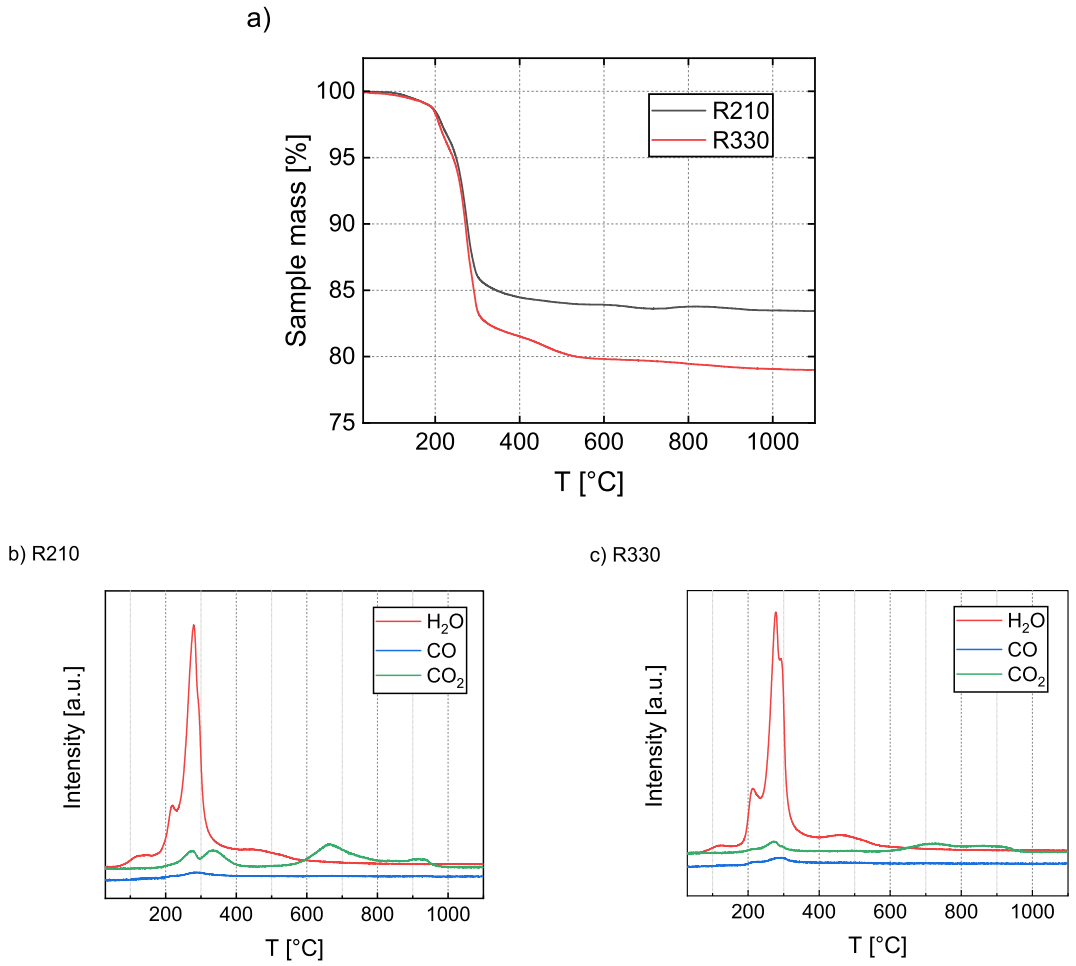

Fig. 12. a) TGA profiles of the used catalyst samples of R210 and R330 after SR of the gas produced from 8 wt% EtOH SCWG at 740 °C with a constant catalyst mass of 2 g and 30 bar, b) MS signals of water vapor and carbon oxides of the R210 used catalyst sample and b) MS signals of water vapor and carbon oxides of the R330 used catalyst.

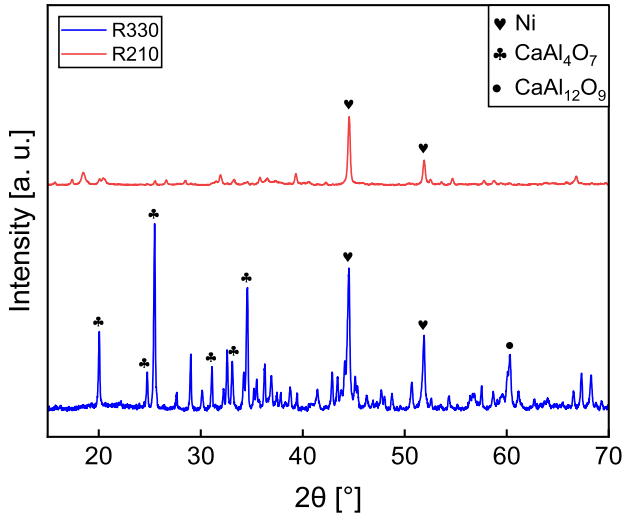

Fig. 13. X-ray diffractograms of used catalysts at SR with 740 °C, catalyst mass of 2 g, and a pressure of 30 bar (SCWG conditions: 600 °C, 265 bar, EtOH in the feed was 8 wt%).

are required to depict the effect of sintering on the stability of both catalysts. Future research will address this by also aiming to overcome any technical hurdles associated with the continuous operation of the process.

4. Conclusions

A continuous process combining the SCWG of EtOH with the subsequent steam reforming of the product gas is demonstrated through an experimental study that involved the operating parameters in the SR reactor, the EtOH concentration, and a comparison of two commercial Ni-based catalysts for the SR of the SCWG product gas. The SCWG was carried out at 600 °C and 265 bar with ethanol as a model compound with concentrations ranging from 5 wt% to 20 wt%.

The effects of temperature, pressure, and space velocity of the SR reactor on the hydrocarbons' conversion and hydrogen yield were investigated. High SR pressures, i.e., 20–40 bar, required a temperature of 750 °C to achieve methane conversion higher than 90%. The GHSV significantly affected the performance of the reforming reactor, especially at high pressures, e.g., at 30 bar, where a GHSV in the range of 40000–50000 h^{-1} was needed to keep the methane conversion close to equilibrium. The concentration of EtOH had a crucial role in the product gas of the combined SCWG-SR process. The increase in EtOH concentration affected the SCWG product by significantly decreasing its S/C ratio, but also increasing the content of CH_4, C_{2+} hydrocarbons, and CO. As a result, SMR and WGS were shifted towards their reactants' side,

decreasing CH_4 conversion from 97.5% to 22.5% and H_2 yield from 98.6% to 58.3%, as the EtOH concentration increased from 5 wt% to 20 wt%. Despite the significant decrease in the S/C ratio and the change in the SCWG product gas composition, between 5 wt% and 20 wt% EtOH, there was a minor carbon formation on both catalysts and not any considerable difference in the Ni sintering rate, under short TOS. Two different commercial catalysts were tested, a NiO(14 wt%)/$CaAl_{12}O_9$ (R330) and a NiO(18 wt%)/$CaK_2Al_{22}O_{34}$ (R210). Both catalysts were under diffusion control at atmospheric pressure, demonstrating almost the same CH_4 conversion. At high SR pressures (30–40 bar), where both catalysts were under kinetic control, the catalyst with the higher Ni loading (R210) showed higher activity. The NiO(18 wt%)/$CaK_2Al_{22}O_{34}$ catalyst resulted in higher sintering rate than the NiO(14 wt %)/$CaAl_{12}O_9$ but the final Ni crystallite size after testing was almost similar for both catalysts. Nevertheless, the former catalyst remained more active than the latter because of the higher Ni loading. The very low coke deposition over both catalysts even under high pressure revealed the resistance to coking mostly due to the excess steam and the high basicity of their supports.

This study verified the possibility of obtaining high hydrogen yields from the SCWG product gas by coupling it with a downstream steam reforming process. Out of the two tested catalysts, the NiO(18 wt %)/$CaK_2Al_{22}O_{34}$ showed to be a suitable catalyst for this specific SR process. Still, its long-term stability has to be further studied and compared with the R330 and other suitable catalysts that offer strong resistance to active metal sintering. Optimizing existing catalyst formulations to enhance their activity and stability in this process will be an important direction for future research. Moreover, future work should prioritize the exploration of alternative feedstocks, focusing on more complex waste biomass model compounds or, ideally, actual waste biomass.

CRediT authorship contribution statement

Athanasios A. Vadarlis: Writing – original draft, Visualization, Software, Methodology, Investigation, Formal analysis, Data curation, Conceptualization. **Dominik Neukum:** Visualization, Validation, Investigation, Formal analysis, Data curation. **Julian Dutzi:** Validation, Methodology, Investigation, Conceptualization. **Angeliki A. Lemonidou:** Writing – review & editing, Validation, Supervision, Investigation, Formal analysis, Data curation, Conceptualization. **Nikolaos Boukis:** Writing – review & editing, Supervision, Resources, Project administration, Funding acquisition, Conceptualization. **Jörg Sauer:** Writing – review & editing, Supervision, Resources, Project administration, Funding acquisition, Formal analysis, Conceptualization.

Funding

The experimental work was supported by the research project: Helmholtz European Partnership for Technological Advancement (HEPTA) [grant agreement no. PIE-0016].

Declaration of competing interest

The authors declare that they have no known competing financial interests or personal relationships that could have appeared to influence the work reported in this paper.

Acknowledgements

The authors would like to thank Mrs. E. Hauer for her contributions to the experimental work and Mr. K. Weiss for his contributions to the mechanical work.

Appendix A. Supplementary data

Supplementary data to this article can be found online at https://doi.org/10.1016/j.ijhydene.2025.02.197.

References

[1] Zimmerman JB, Anastas PT, Erythropel HC, Leitner W. Science 2020;367(6476):397–400. https://doi.org/10.1126/science.aay3060. 1979.
[2] Shaw WJ, Kidder MK, Bare SR, Delferro M, Morris JR, Toma FM, Senanayake SD, Autrey T, Biddinger EJ, Boettcher S, et al. Nat Rev Chem 2024;8(5):376–400. https://doi.org/10.1038/s41570-024-00587-1.
[3] Erans M, Sanz-Pérez ES, Hanak DP, Clulow Z, Reiner DM, Mutch GA. Energy Environ Sci 2022;15(4):1360–405. https://doi.org/10.1039/D1EE03523A.
[4] Bram MV, Liniger J, Majidabad SS, Shabani HR, Teles MPR, Cui X. Int J Hydrogen Energy 2024. https://doi.org/10.1016/j.ijhydene.2024.05.273.
[5] Nnabuife SG, Ugbeh-Johnson J, Okeke NE, Ogbonnaya C. Carbon Capture Sci Technol 2022;3:100042. https://doi.org/10.1016/j.ccst.2022.100042.
[6] Berchthold C, Geisbauer A. Monatsh Chem 2024. https://doi.org/10.1007/s00706-024-03176-6.
[7] Antzaras AN, Lemonidou AA. Renew Sustain Energy Rev 2022;155:111917. https://doi.org/10.1016/j.rser.2021.111917.
[8] Rostrup-Nielsen JR, Sehested J, Nørskov JK. Advances in catalysis, vol. 47. Academic Press; 2002.
[9] Rostrup-Nielsen JR. In: Anderson JR, Boudart M, editors. Catalysis, vol. 5. Berlin, Heidelberg: Springer; 1984.
[10] Pinaeva LG, Noskov AS. Catalogue Index 2022;14(1):66–85. https://doi.org/10.1134/S2070050422010081.
[11] Fowles M, Carlsson M. Top Catal 2021;64(17–20):856–75. https://doi.org/10.1007/S11244-021-01496-Z/FIGURES/19.
[12] Angeli SD, Pilitsis FG, Lemonidou AA. Catal Today 2015;242:119–28. https://doi.org/10.1016/j.cattod.2014.05.043. Part A.
[13] Pashchenko D. Int J Hydrogen Energy 2019;44(59):30865–75. https://doi.org/10.1016/j.ijhydene.2019.10.009.
[14] Pashchenko D, Gnutikova M, Karpilov I. Int J Hydrogen Energy 2020;45(7):4174–81. https://doi.org/10.1016/j.ijhydene.2019.11.202.
[15] Zhu Y, He Z, Xuan T, Huang Y, Zhong W. Fuel 2024;378:132767. https://doi.org/10.1016/J.FUEL.2024.132767.
[16] Vogt ETC, Weckhuysen BM. Nature 2024;629(8011):295–306. https://doi.org/10.1038/s41586-024-07322-2.
[17] Kullmann F, Linßen J, Stolten D. Int J Hydrogen Energy 2023;48(99):38936–52. https://doi.org/10.1016/J.IJHYDENE.2023.04.191.
[18] Rodriguez Correa C, Kruse A. J Supercrit Fluids 2018;133:573–90. https://doi.org/10.1016/j.supflu.2017.09.019.
[19] Jeje SO, Marazani T, Obiko JO, Shongwe MB. Int J Hydrogen Energy 2024;78:642–61. https://doi.org/10.1016/J.IJHYDENE.2024.06.344.
[20] Shahbaz M, Al-Ansari T, Aslam M, Khan Z, Inayat A, Athar M, Naqvi SR, Ahmed MA, McKay G. Int J Hydrogen Energy 2020;45(30):15166–95. https://doi.org/10.1016/J.IJHYDENE.2020.04.009.
[21] Ferreira-Pinto L, Silva Parizi MP, Carvalho de Araújo PC, Zanette AF, Cardozo-Filho L. Int J Hydrogen Energy 2019;44(47):25365–83. https://doi.org/10.1016/j.ijhydene.2019.08.023.
[22] Lee CS, Conradie AV, Lester E. Chem Eng J 2021;415:128837. https://doi.org/10.1016/j.cej.2021.128837.
[23] Su H, Yan M, Wang S. Renew Sustain Energy Rev 2022;154:111831. https://doi.org/10.1016/J.RSER.2021.111831.
[24] Peterson AA, Vogel F, Lachance RP, Fröling M, Antal MJ, Tester JW. Energy Environ Sci 2008;1(1):32–65. https://doi.org/10.1039/B810100K.
[25] Dutzi J, Boukis N, Sauer J. Processes 2023;11(3):797. https://doi.org/10.3390/PR11030797. 2023, Vol. 11, Page 797.
[26] Matsumura Y, Minowa T, Potic B, Kersten SRA, Prins W, Van Swaaij WPM, Van De Beld B, Elliott DC, Neuenschwander GG, Kruse A, et al. Biomass Bioenergy 2005;29(4):269–92. https://doi.org/10.1016/j.biombioe.2005.04.006.
[27] Brito J, Pinto F, Ferreira A, Soria MA, Madeira LM. Fuel Process Technol 2023;250:107859. https://doi.org/10.1016/j.fuproc.2023.107859.
[28] Vadarlis AA, Neukum D, Lemonidou AA, Boukis N, Sauer J. Int J Hydrogen Energy 2024;49:992–1008. https://doi.org/10.1016/j.ijhydene.2023.08.108.
[29] N. Boukis, I. K. Stoll, 2021. DOI: 10.3390/pr9030455.
[30] Hantoko D, Su H, Yan M, Kanchanatip E, Susanto H, Wang G, Zhang S, Xu Z. Int J Hydrogen Energy 2018;43(37):17620–32. https://doi.org/10.1016/j.ijhydene.2018.07.198.
[31] Kumar M, Oyedun AO, Kumar A. Int J Hydrogen Energy 2019;44(21):10384–97. https://doi.org/10.1016/j.ijhydene.2019.02.220.
[32] Rahbari A, Shirazi A, Venkataraman MB, Pye J. Appl Energy 2021;288:116620. https://doi.org/10.1016/j.apenergy.2021.116620.
[33] Ruya PM, Lim SS, Purwadi R, Zunita M. Energy 2020:208. https://doi.org/10.1016/j.energy.2020.118280.
[34] Campanario FJ, Gutiérrez Ortiz FJ. Energy Convers Manag 2017;150:599–613. https://doi.org/10.1016/j.enconman.2017.08.053.
[35] Zhang C, Li Y, Chu Z, Fang Y. Energy Convers Manag 2023;278:116710. https://doi.org/10.1016/j.enconman.2023.116710.
[36] Lemonidou AA, Goula MA, Vasalos IA. Catal Today 1998;46(2–3):175–83. https://doi.org/10.1016/S0920-5861(98)00339-3.

[37] Goula MA, Lemonidou AA, Grünert W, Baerns M. Catal Today 1996;32(1–4):149–56. https://doi.org/10.1016/S0920-5861(96)00168-X.
[38] Angeli SD, Turchetti L, Monteleone G, Lemonidou AA. Appl Catal, B 2016;181:34–46. https://doi.org/10.1016/j.apcatb.2015.07.039.
[39] Pirzadi Z, Meshkani F, Vo DVN. Energy Convers Manag 2024;311:118227. https://doi.org/10.1016/J.ENCONMAN.2024.118227.
[40] Fernandez E, Santamaria L, Artetxe M, Amutio M, Arregi A, Lopez G, Bilbao J, Olazar M. Fuel 2022;312:122910. https://doi.org/10.1016/j.fuel.2021.122910.
[41] Lopez G, Erkiaga A, Artetxe M, Amutio M, Bilbao J, Olazar M. Ind Eng Chem Res 2015;54(39):9536–44. https://doi.org/10.1021/ACS.IECR.5B02413.
[42] Erkiaga A, Lopez G, Barbarias I, Artetxe M, Amutio M, Bilbao J, Olazar M. J Anal Appl Pyrolysis 2015;116:34–41. https://doi.org/10.1016/j.jaap.2015.10.010.
[43] Sabokmalek S, Alavi SM, Rezaei M, Akbari E. J Energy Inst 2023;109:101270. https://doi.org/10.1016/J.JOEI.2023.101270.
[44] Arita T, Nakahara K, Nagami K, Kajimoto O. Tetrahedron Lett 2003;44(5):1083–6. https://doi.org/10.1016/S0040-4039(02)02704-1.
[45] B Kistiakowsky BG, Romeyn H, Ruhoff JR, Smith HA, Vaughan WE. Heats of organic reactions. I. The apparatus and the heat of hydrogenation of ethylene, vol. 16. UTC; 2023.
[46] Dutzi J, Vadarlis AA, Boukis N, Sauer J. Ind Eng Chem Res 2023;62(32):12501–12. https://doi.org/10.1021/acs.iecr.3c01595.
[47] Kruse A, Meier D, Rimbrecht P, Schacht M. Ind Eng Chem Res 2000;39(12):4842–8. https://doi.org/10.1021/ie0001570.
[48] Sheikhdavoodi MJ, Almassi M, Ebrahimi-Nik M, Kruse A, Bahrami H. J Energy Inst 2015;88(4):450–8. https://doi.org/10.1016/J.JOEI.2014.10.005.
[49] Onwudili JA, Lea-Langton AR, Ross AB, Williams PT. Bioresour Technol 2013;127:72–80. https://doi.org/10.1016/J.BIORTECH.2012.10.020.
[50] Xu ZR, Zhu W, Gong M, Zhang HW. Int J Hydrogen Energy 2013;38(10):3963–72. https://doi.org/10.1016/J.IJHYDENE.2013.01.164.
[51] Byrd AJ, Pant KK, Gupta RB. Energy Fuel 2007;21(6):3541–7. https://doi.org/10.1021/ef700269z.
[52] Voll FAP, Rossi CCRS, Silva C, Guirardello R, Souza ROMA, Cabral VF, Cardozo-Filho L. Int J Hydrogen Energy 2009;34(24):9737–44. https://doi.org/10.1016/J.IJHYDENE.2009.10.017.
[53] Angeli SD, Monteleone G, Giaconia A, Lemonidou AA. Int J Hydrogen Energy 2014;39(5):1979–97. https://doi.org/10.1016/j.ijhydene.2013.12.001.
[54] Zhao Q, Wang Y, Wang Y, Li L, Zeng W, Li G, Hu C. Int J Hydrogen Energy 2020;45(28):14281–92. https://doi.org/10.1016/j.ijhydene.2020.03.112.
[55] Sperle T, Chen D, Lødeng R, Holmen A. Appl Catal Gen 2005;282(1–2):195–204. https://doi.org/10.1016/j.apcata.2004.12.011.
[56] Choi S, Bae J, Lee S, Oh J, Katikaneni SP. Chem Eng Sci 2017;168:15–22. https://doi.org/10.1016/j.ces.2017.04.033.
[57] Palma V, Ricca A, Meloni E, Martino M, Miccio M, Ciambelli P. J Clean Prod 2016;111:217–30. https://doi.org/10.1016/j.jclepro.2015.09.004.
[58] Wang S, Shen Z, Osatiashtiani A, Nabavi SA, Clough PT. Chem Eng J 2024;486:150170. https://doi.org/10.1016/j.cej.2024.150170. November 2023.
[59] Wang Y, Yoshiba F, Kawase M, Watanabe T. Int J Hydrogen Energy 2009;34(9):3885–93. https://doi.org/10.1016/J.IJHYDENE.2009.02.073.
[60] Abbas SZ, Dupont V, Mahmud T. Int J Hydrogen Energy 2017;42(5):2889–903. https://doi.org/10.1016/J.IJHYDENE.2016.11.093.
[61] Sehested J, Gelten JAP, Helveg S. Appl Catal Gen 2006;309(2):237–46. https://doi.org/10.1016/J.APCATA.2006.05.017.
[62] Christensen KO, Chen D, Lødeng R, Holmen A. Appl Catal Gen 2006;314(1):9–22. https://doi.org/10.1016/j.apcata.2006.07.028.
[63] Xu J, Yeung CMY, Ni J, Meunier F, Acerbi N, Fowles M, Tsang SC. Appl Catal Gen 2008;345(2):119–27. https://doi.org/10.1016/J.APCATA.2008.02.044.
[64] Roy PS, Raju ASK, Kim K. Fuel 2015;139:314–20. https://doi.org/10.1016/J.FUEL.2014.08.062.
[65] Vannice MA. Kinetics of catalytic reactions. Springer Science+Business Media, Inc; 2005.
[66] Khavarian M, Chai SP, Mohamed AR. Chem Eng J 2014;257:200–8. https://doi.org/10.1016/j.cej.2014.05.079.
[67] Sidjabat O, Trimm DL. Top Catal 2000;11–12(1–4):279–82. https://doi.org/10.1023/A:1027212301077.
[68] Meshkani F, Golesorkh SF, Rezaei M, Andache M. Res Chem Intermed 2017;43(1):545–59. https://doi.org/10.1007/s11164-016-2639-z.
[69] Keshavarz AR, Soleimani M. Res Chem Intermed 2018;44(3):1485–503. https://doi.org/10.1007/S11164-017-3180-4/FIGURES/12.
[70] Hashemnejad SM, Parvari M. Chin J Catal 2011;32(1–2):273–9. https://doi.org/10.1016/S1872-2067(10)60175-1.
[71] Christensen KO, Chen D, Lødeng R, Holmen A. Appl Catal Gen 2006;314(1):9–22. https://doi.org/10.1016/J.APCATA.2006.07.028.
[72] Mears DE. Ind Eng Chem Process Des Dev 1970;10(8):397.
[73] Jiang B, Zhang C, Wang K, Dou B, Song Y, Chen H, Xu Y. Appl Therm Eng 2016;109:99–108. https://doi.org/10.1016/J.APPLTHERMALENG.2016.08.041.
[74] Bangala DN, Abatzoglou N, Chornet E. AIChE J 1998;44(4):927–36. https://doi.org/10.1002/aic.690440418.
[75] Garbarino G, Pugliese F, Cavattoni T, Busca G, Costamagna P. Energies 2020;13(11). https://doi.org/10.3390/en13112792.
[76] Parizotto NV, Rocha KO, Damyanova S, Passos FB, Zanchet D, Marques CMP, Bueno JMC. Appl Catal Gen 2007;330:12–22. https://doi.org/10.1016/j.apcata.2007.06.022.
[77] Bao Z, Lu Y, Han J, Li Y, Yu F. Appl Catal Gen 2015;491:116–26. https://doi.org/10.1016/j.apcata.2014.12.005.
[78] Chatterjee R, Banerjee S, Banerjee S, Ghosh D. Trans Indian Inst Met 2012;65(3):265–73. https://doi.org/10.1007/s12666-012-0130-0.